

# Observation of a new high-energy, shallow-bound Rydberg state in $I_2$ by optical triple resonance

A. Marica Sjödin<sup>1</sup>, Trevor Ridley<sup>\*</sup>, Kenneth P. Lawley, Robert J. Donovan

*School of Chemistry, The University of Edinburgh, West Mains Road, Edinburgh EH9 3JJ, Scotland, UK*

Received 9 May 2005; in final form 24 June 2005

Available online 18 July 2005

## Abstract

A new  $0_u^+$  6s Rydberg state built on an excited ionic core of  $I_2$  has been observed by optical triple resonance via the  $B(0_u^+)$  valence and  $E0_g^+(^3P_2)$  ion-pair states with ionization detection. A vibrational progression,  $v = 0-27$ , was observed for selected rotational levels and molecular constants are presented. The Rydberg state is weakly bound and was determined to have an internuclear separation of  $4.500 \pm 0.003$  Å.

© 2005 Elsevier B.V. All rights reserved.

## 1. Introduction

Rydberg states built on electronically excited ion core states give rise to structure in the ionization cross-section of molecules, where they result in autoionization and ion-pair formation. Yenchu et al. [1] observed such structure in  $I_2$  above the threshold of the upper spin-orbit component,  $X(^2\Pi_{g,1/2})$ , of the ground state of the molecular ion and assigned it to Rydberg states converging on the  $A(^2\Pi_u)$  limit and on an unidentified higher state of  $I_2^+$ . During an investigation of ion-pair formation from photodissociation in  $I_2$ , Kvaran et al. [2] observed clearly resolved structure in the  $I^+$ ,  $I^-$  and  $I_2^+$  channels slightly below the onset for  $I_2^+X(^2\Pi_{g,1/2})$  and assigned this as being due to an  $A[^2\Pi_{u,3/2}]_c8s$  Rydberg state.

Depending on the energy of the excited core state, these Rydberg series may begin below the first IE, but reports of observations of such states that are not auto-

ionizing are sparse. Two strong progressions in the vacuum ultraviolet (VUV) absorption spectrum of  $Br_2$  have been assigned as the  $A[^2\Pi_{1/2,3/2}]_c5s;1_u$  Rydberg states [3]. Some series of Rydberg states built on  $N_2^+A(^2\Pi_u)$  have been observed both above and below the first IE. An analysis and overview of these states is given by Lefebvre-Brion and Yoshino [4] and also by Huber et al. [5].

In  $I_2$ , several 6s and 6p Rydberg states built on excited states of  $I_2^+$  are predicted to lie, entirely or partly, below the first IE. Some bands in the VUV absorption spectrum were assigned to these states [6]. However, in a subsequent re-assignment [3] of that spectrum, all of the bands in question were assigned to Rydberg states built on the ground state of the ion.

Excited ion core Rydberg states are expected to have poor Franck–Condon overlap with the ground state (the equilibrium bond lengths of the electronically excited states of  $I_2^+$  are estimated to be in the range 3.0–3.5 Å compared to 2.66 Å for  $I_2 X(0_g^+)$ , so these states are more likely to be observed using a multi-stage excitation scheme which extends the accessible radial region to larger internuclear separation. In recent papers [7,8], we have reported studies of the high-energy region of  $I_2$  using optical triple resonance together with resonance ionization (OTR/RI). Our broad aim is to study the

<sup>\*</sup> Corresponding author. Fax: +44 131 650 6453.

E-mail address: [T.Ridley@ed.ac.uk](mailto:T.Ridley@ed.ac.uk) (T. Ridley).

<sup>1</sup> Also at: Department of Physics, Section of Atomic and Molecular Physics, Royal Institute of Technology, KTH Roslagstullsbacken 21, S-106 91 Stockholm, Sweden.

high-energy region, including the core excited Rydberg states of  $I_2$  and other halogens. In the typical OTR scheme used, the  $E0_g^+(^3P_2)$  ion-pair state was optically accessed via the  $B(0_u^+)$  valence state in a rotationally selective double resonance scheme using two pump photons of different energy;  $\nu_1$  for the  $B(0_u^+) \leftarrow X(0_g^+)$  transition and  $\nu_2$  for the  $E0_g^+(^3P_2) \leftarrow B(0_u^+)$  transition. A third photon,  $\nu_3$ , was scanned to probe the energy region around or below the first ion-pair dissociation threshold of  $I_2$ . The OTR excitation scheme opens a different and wider Franck–Condon window than coherent excitation from the ground state or even double resonance via the  $B(0_u^+)$  valence state. The resonant pumping scheme of this multiphoton process also allows us to probe energy states in the VUV region using relatively low intensities.

The OTR/RI spectrum of  $I_2$  in the energy range 60 300–65 800  $\text{cm}^{-1}$  is heavily perturbed [8]. We have identified many vibrational levels of a  $0_u^+$  Rydberg state. However, both rotational and vibrational separations vary throughout the vibrational progression due to interactions both with ion-pair states and at least one Rydberg state built on the ground state of  $I_2^+$ , making the observed state difficult to characterize. By contrast, when the OTR/RI spectrum is extended to higher energy we see a second vibrational progression that is remarkably regular. In this Letter, we present the spectroscopic constants determined for the upper vibrational progression and begin a discussion of the nature of the state.

## 2. Experimental

The experimental arrangement used to record the OTR/RI spectra has been described in detail elsewhere [8]. Briefly, it comprised a laser system with three tunable, excimer-pumped dye lasers, a pulsed molecular beam, a time-of-flight mass spectrometer and signal collection electronics. The  $\nu_2$  and  $\nu_3$  photons were introduced collinearly into the differentially pumped ionization chamber via a 6-cm focal length lens. The  $\nu_1$  photons were directed into the chamber at  $180^\circ$  to the other two beams and similarly focussed to an overlapping point. The counter-propagating dye laser beams intersected the molecular beam at  $90^\circ$  between two electrodes separated by a distance of 1.6 cm. Ions were collected via a 52-cm long flight tube which was terminated by a microchannel plate detector. The pulsed jet was of conventional design and employed a commercial pulsed valve (General Valve, nozzle diameter 250  $\mu\text{m}$ ). Helium at a pressure of 300–500 Torr (depending on the desired temperature of the molecular beam) was passed over solid  $I_2$  at room temperature and the resulting mixture of  $I_2$  and carrier gas expanded through the nozzle which was warmed to  $\sim 310$  K.

The dyes used were C153 for  $\nu_1$ , DMQ for  $\nu_2$  and C2 for  $\nu_3$ . The probe laser wavelength was calibrated from neon optogalvanic lines, resulting in absolute errors of  $\sim 0.3$   $\text{cm}^{-1}$ . The first pump step was identified from the  $I_2$  fluorescence excitation spectrum and the second pump step had previously been ascertained through calibration against neon optogalvanic lines. The total energy of observed states was obtained by adding the calibrated energy of the probe photon to the energy of the pumped rovibrational level of the  $E0_g^+(^3P_2)$  state calculated from known molecular constants [9]. As the stated uncertainty of the calculated levels of the  $E0_g^+(^3P_2)$  state is  $0.033$   $\text{cm}^{-1}$ , the error in total energy is assumed to be dominated by the experimental uncertainty of the measured probe energy. Throughout the present Letter, we will use the term ‘total energy’ which is given relative to  $X(0_g^+)$  ( $v = 0, J = 0$ ).

The excitation pathway is illustrated in Fig. 1. For clarity, since two intermediate states are used, the vibrational and rotational labels are identified by the electronic label of the state. The first pump photon,  $\nu_1$ , was set to selected rotational branches of the (22, 0) band of the  $B(0_u^+) \leftarrow X(0_g^+)$  transition [10]. For all overview spectra, the overlapping P(25) and R(29) branches were pumped and hence ( $J_B = 24$  and 30) are both excited. The second (intermediate) pump photon,  $\nu_2$ , was then tuned to the R(24) branch of various ( $v_E, 22$ ) bands of the  $E0_g^+(^3P_2) \leftarrow B(0_u^+)$  transition and hence ( $v_E, J_E = 25$ ), uniquely, was excited. During the experiment, several different vibrational levels of the  $E0_g^+(^3P_2)$  state were pumped; i.e.,  $v_E = 41, 46, 51$  and 53. Finally, the

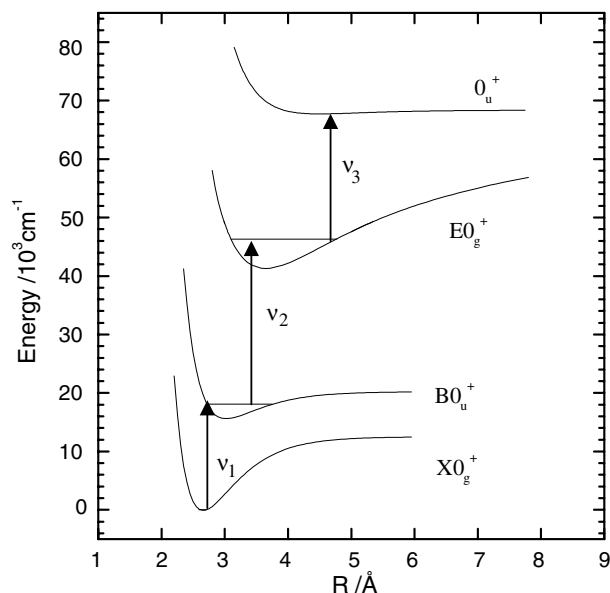


Fig. 1. The OTR excitation pathway. The new Rydberg state is indicated by a Morse fit of the experimental data assuming dissociation to  $I(^2P_{3/2}) + I^*(^3P_{2k}6s; ^2P_{3/2})$ . The vibrational levels indicated are ( $v_E = 53$ ) and ( $v_B = 22$ ).

probe photon,  $\nu_3$ , was scanned between 438 and 472 nm exciting transitions from the  $E0_g^+(^3P_2)$  state to a higher lying state, which was then ionized by absorption of at least one more photon. The spectra were recorded by monitoring  $I^+$ , as the spectra observed by monitoring  $I_2^+$  were much weaker.

The potential function for the new state in Fig. 1 is modelled by a Morse curve based on the experimental data (this will be discussed in more detail below). From this potential, it is clear that transitions to bound levels of the final state occur near the outer turning point of the  $E0_g^+(^3P_2)$  state.

### 3. Results

An overview of the OTR/RI spectra over the total energy region 67 500–68 350  $\text{cm}^{-1}$  recorded via ( $v = 53$ ,  $J = 25$ ) and ( $v = 51$ ,  $J = 25$ ) of the  $E0_g^+(^3P_2)$  state are shown in Fig. 2. Both spectra show a vibrational progression, with  $J = 24$  and 26, beginning at 67 722  $\text{cm}^{-1}$  and this is assigned as the ( $v = 0$ ) level. This level was also the lowest in spectra recorded via ( $v = 41$ ) and ( $v = 46$ ) of the  $E0_g^+(^3P_2)$  state, confirming the ( $v = 0$ ) assignment. The progression extends from  $v = 0$ –27, during which the vibrational separation decreases from 33 to 12  $\text{cm}^{-1}$ . A few higher vibrational levels of the  $E0_g^+(^3P_2)$  state were used in an attempt to improve the Franck–Condon overlap with higher vibrational levels of the final state, but no further levels were seen. We have seen some indication of interaction with another electronic state above 68 300  $\text{cm}^{-1}$  and this is the probable cause of the loss of signal.

Throughout the spectrum only P and R doublets, indicative of parallel one-photon transitions, were seen.

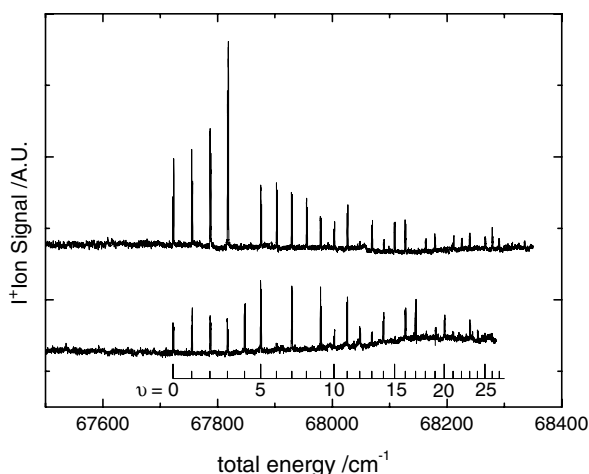


Fig. 2. An overview of the OTR/RI spectrum of  $I_2$  over the total energy range 67 500–68 350  $\text{cm}^{-1}$ . The upper spectrum was recorded via ( $v = 53$ ,  $J = 25$ ) of the  $E0_g^+(^3P_2)$  state and the lower spectrum was recorded via ( $v = 51$ ,  $J = 25$ ) of the same state. Total energy is given relative to  $X$  ( $v = 0$ ,  $J = 0$ ).

This identifies the symmetry of the new state as  $0_u^+$ . The rotational splitting between  $J = 24$  and 26 of  $\sim 1.3 \text{ cm}^{-1}$  indicates an internuclear separation of  $\sim 4.6 \text{ \AA}$ . The small vibrational and rotational separations and the energy region could be indicative of high vibrational levels of an ion-pair state ( $F'0_u^+(^1D_2)$   $v \sim 200$ ). However, the  $I^+(^1D_2) + I^-(^1S)$  ion-pair dissociation limit lies at 85 790  $\text{cm}^{-1}$  and the vibrational progression in Fig. 2 converges far too rapidly to go even as high as the first ion-pair formation threshold  $I^+(^3P_2) + I^-(^1S)$  at 72 060  $\text{cm}^{-1}$ . So, we can rule out this possibility and hence the state must be a Rydberg state.

The spectra in Fig. 2 are composites of several scans. No attempt has been made to normalize the spectra for variation in the probe intensity. However, the OTR spectra were recorded using the middle of the spectral range of the dye C2, so local relative intensities and missing vibrational levels are determined by Franck–Condon factors and are not due to variations in dye laser power. In addition, it is immediately apparent that vibrational levels that are missing in one spectrum are clearly present in the spectrum recorded via a different  $v_E$  and hence the intensity variations are not caused by predissociation of the upper state levels.

Rotational data of the new  $0_u^+$  state was obtained by changing the pumping scheme to populate different rotational levels of  $E0_g^+(^3P_2)$  ( $v_E = 53$ ). The first photon,  $\nu_1$ , pumps the (22, 0) band of the  $B(0_u^+) \leftarrow X(0_g^+)$  transition. Within the range  $J_X = 9$ –33, the rotational branches  $P(J_X)$  and  $R(J_X + 4)$  are separated by less than 0.02  $\text{cm}^{-1}$ , within the resolution of the pump laser, and so  $\nu_1$  pumps an overlapping P/R pair. The congestion near the band head made  $P(9)/R(13)$  the lowest pair of lines that could be uniquely pumped. The population of high  $J$  levels in the cooled molecular beam was increased by using a lower backing pressure. This, however, also decreased the amount of sample in the ionization region and as a result the signal became weaker for increasing  $J$  and we did not pursue levels above  $J = 33$ . Since two rotational levels are populated in the  $B(0_u^+)$  state ( $J_B$  and  $J_B + 6$ ) there exists the possibility of pumping four different branches in the second step. We chose to use only the two well separated  $R(J_B)$  and  $P(J_B + 6)$  branches. Thus, two OTR spectra were recorded for every  $\nu_1$  used; each spectrum was pumped via a single rovibrational level of the  $E0_g^+(^3P_2)$  state and hence shows two rotational levels of the final state.

The most extensive set of data was obtained for  $v = 0$  of the new  $0_u^+$  state where four separate P/R pairs of the (22,0) band of the  $B(0_u^+) \leftarrow X(0_g^+)$  transition were pumped;  $P(9)/R(13)$ ,  $P(18)/R(22)$ ,  $P(25)/R(29)$  and  $P(33)/R(37)$ . The resulting spectra are shown in Fig. 3. A more limited study using  $P(18)/R(22)$  and  $P(25)/R(29)$  was carried out for twelve vibrational levels between 1 and 27. For all of these vibrational levels,

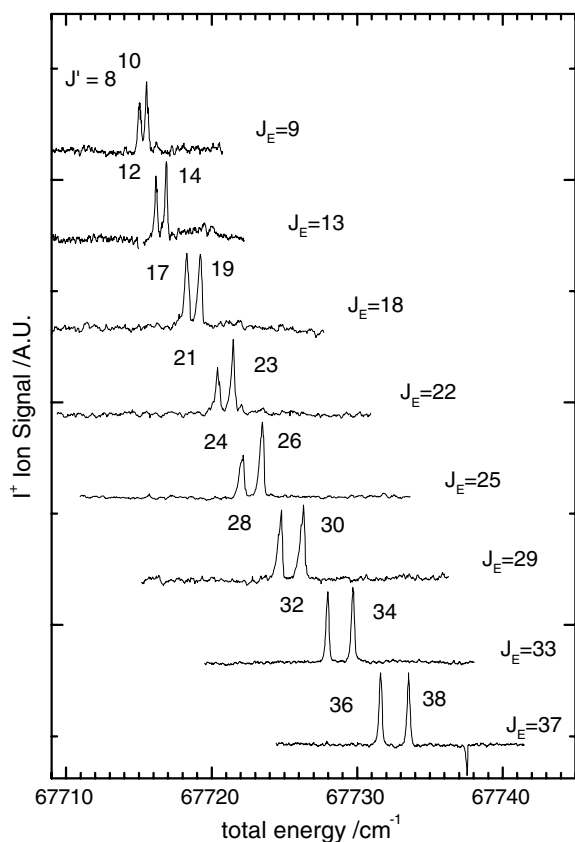


Fig. 3. Observed rotational levels of ( $v=0$ ) of the  $0_u^+$  state. The label  $J_E$  refers to the rotational levels of  $E0_g^+(^3P_2)$  ( $v_E=53$ ) that were populated.

the total energy of the eight observed rotational levels (16 levels for  $v=0$ ) produced straight line fits when plotted vs.  $J(J+1)$ , thus giving  $G_v$  and  $B_v$  for the 13 vibrational levels. These values were in turn fitted as functions of  $(v+1/2)$  to produce, respectively, the vibrational constants  $T_e$ ,  $\omega_e$ ,  $\omega_e x_e$  and  $\omega_e y_e$  and the rotational constants  $B_e$ ,  $\alpha_e$  and  $\gamma_e$  and these are presented in Table 1. A higher order term than  $\gamma_e$  was not found to be necessary. Although these constants were not obtained through a global fit, they reproduce all 144 observed levels to within  $0.5 \text{ cm}^{-1}$ . Both rotational and vibrational levels are remarkably regular. Even for  $v \sim 27$  any deviations from the linear fit in the rotational levels were within experimental errors. The resulting  $B_v$  values fitted well to a second order polynomial. The vibrational constants for  $\omega_e$ ,  $\omega_e x_e$  and  $\omega_e y_e$  obtained from the fit of the

Table 1  
Molecular constants for the  $0_u^+$  Rydberg state

$T_e$	$67697.3 \pm 0.1 \text{ cm}^{-1}$
$\omega_e$ ( $\sim Y_{10}$ )	$34.08 \pm 0.05 \text{ cm}^{-1}$
$\omega_e x_e$ ( $\sim Y_{20}$ )	$0.587 \pm 0.005 \text{ cm}^{-1}$
$\omega_e y_e$ ( $\sim Y_{30}$ )	$0.00457 \pm 0.00013 \text{ cm}^{-1}$
$B_e \times 10^2$ ( $\sim Y_{01}$ )	$1.312 \pm 0.002 \text{ cm}^{-1}$
$\alpha_e \times 10^5$ ( $\sim Y_{11}$ )	$4.8 \pm 0.6 \text{ cm}^{-1}$
$\gamma_e \times 10^6$ ( $\sim Y_{12}$ )	$-3.7 \pm 0.3 \text{ cm}^{-1}$
$R_e$	$4.500 \pm 0.003 \text{ \AA}$

$G_v$  values were almost the same as the constants obtained from a fit of ( $J=24$ ) or ( $J=26$ ) of all vibrational levels. In both cases the fit was improved by including the  $\omega_e y_e$  term.

A Morse potential, calculated using  $T_e$ ,  $\omega_e$  and  $\omega_e x_e$  ( $67698.7$ ,  $32.595$  and  $0.416 \text{ cm}^{-1}$ ) obtained from a fit of the experimental data without including an  $\omega_e y_e$  term, has a dissociation limit of  $68337 \text{ cm}^{-1}$ . The three nearest  $I_{\text{val}} + I_{\text{Ryd}}$  dissociation limits are  $^2P_{3/2} + [^3P_2]_c 6s; ^4P_{5/2}$ ,  $^2P_{3/2} + [^3P_2]_c 6s; ^2P_{3/2}$  and  $^2P_{3/2} + [^3P_0]_c 6s; ^4P_{1/2}$  lying at  $67073$ ,  $68532$  and  $73336 \text{ cm}^{-1}$ , respectively [11,12]. Although the new Rydberg state cannot be accurately described by a Morse potential, it is still clear from such a potential that the state must correlate with the second of these dissociation limits.

The constants in Table 1 have been used to calculate the RKR potential that is illustrated in Fig. 4 and the turning points of which are given in Table 2. Fig. 4 also indicates the only two dissociation limits in this energy region, confirming that the state must correlate with the higher of the two. The new state is broad and weakly bound with a  $D_e$  of only  $835 \text{ cm}^{-1}$  (cf.  $638 \text{ cm}^{-1}$  estimated from a Morse function) which means that the observed vibrational progression  $v=0-27$  covers 70% of the potential well. Although, as already mentioned, we have seen some sign of interaction with another electronic state above  $v=28$ , below this the spectrum is sharp and regular indicating that the state is long-lived and unperturbed.

The new state is thus a  $6s$  Rydberg state and, from the symmetry,  $T_e$  and  $R_e$ , must be based on an excited state of  $I_2^+$  of ungerade parity. The four lowest energy excited states of  $I_2^+$  that can give rise to an  $ns$ -Rydberg state with a  $0_u^+$  component under  $\Omega, \omega$  coupling are  $a(^4\Sigma_u^-)$ ,  $A(^2\Pi_{u,1/2})$ ,  $^2\Sigma_u^+$  and  $^2\Sigma_u^-$ . The  $a(^4\Sigma_u^-)$  and  $A(^2\Pi_u)$  states have been observed with resolved vibrational structure, although the absolute vibrational

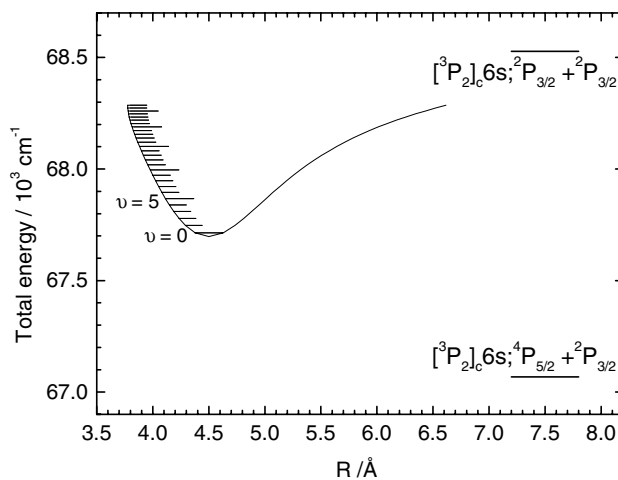


Fig. 4. RKR potential of the  $0_u^+$  state. The two lowest  $6s$  Rydberg dissociation limits are indicated.

Table 2  
RKR potential for the  $0_u^+$  Rydberg state

$v$	$G_v$	$R_{\min}/\text{Å}$	$R_{\max}/\text{Å}$
0	16.9	4.377	4.629
1	49.8	4.292	4.734
2	81.6	4.234	4.813
3	112.3	4.188	4.883
4	141.9	4.148	4.948
5	170.4	4.113	5.011
6	198.0	4.081	5.072
7	224.5	4.052	5.133
8	250.1	4.025	5.194
9	274.7	4.000	5.255
10	298.4	3.977	5.317
11	321.2	3.955	5.379
12	343.2	3.935	5.443
13	364.4	3.916	5.508
14	384.7	3.898	5.575
15	404.3	3.881	5.643
16	423.1	3.865	5.713
17	441.2	3.851	5.785
18	458.6	3.838	5.858
19	475.3	3.826	5.934
20	491.4	3.815	6.012
21	506.9	3.805	6.091
22	521.8	3.797	6.173
23	536.1	3.790	6.257
24	549.9	3.784	6.344
25	563.2	3.780	6.433
26	576.1	3.778	6.524
27	588.5	3.776	6.617

numbering has not been determined. The onset of the vibrational bands in the OODR/ZEKE spectrum recorded by Cockett et al. [13] sets upper limits of 86022 and 86367  $\text{cm}^{-1}$  for the  $a(^4\Sigma_u^-)$  and  $A(^2\Pi_{u,3/2})$  states, respectively, and these were thought to be near the true IEs. The spin-orbit coupling in the  $A(^2\Pi)$  state is  $\sim 6400 \text{ cm}^{-1}$ , obtained from the energy difference between equivalent parts of the photoelectron bands [14], hence the IE for the  $A(^2\Pi_{1/2})$  state is predicted to be  $\sim 92767 \text{ cm}^{-1}$ . Neither the  $^2\Sigma_u^+$  nor the  $^2\Sigma_u^-$  state has been observed and estimations of their IEs from ab initio calculations are inconclusive [15,16].

The effective quantum number,  $n^*$  (i.e.,  $n-\delta$ ), is commonly used to assign Rydberg states. This can be obtained using the conventional Rydberg equation

$$E_n = \text{IE} - R/(n - \delta)^2,$$

where  $E_n$  is the energy of the electronic origin of the Rydberg state, IE is the ionization energy of the appropriate state of the ion and  $\delta$  is the quantum defect. The  $n^*$  of the  $X(^2\Pi_{3/2,1/2})_c;6s$  Rydberg states in  $\text{I}_2$ ,  $\text{ICl}$  and  $\text{IBr}$  have been reported [3,17] to vary only slightly over the range 1.97–2.03. The IEs of the  $a(^4\Sigma_u^-)$  and  $A(^2\Pi_{u,1/2})$  states yield  $n^*$  values of 2.45 and 2.09, respectively, for the origin of the new state. The  $n^*$  value obtained using the IE of the  $a(^4\Sigma_u^-)$  state of  $\text{I}_2^+$  is much too high, hence the Rydberg state cannot have an  $a(^4\Sigma_u^-)$  ionic core.

The  $n^*$  value obtained using the IE of the  $A(^2\Pi_{u,1/2})$  state of  $\text{I}_2^+$  is still rather large but, based on  $n^*$  alone, this remains a possible core for the Rydberg state. However, the vibrational separations in the  $A(^2\Pi_{1/2})$  state have been observed [1] as roughly  $120 \text{ cm}^{-1}$ , much larger than those observed here. Furthermore, the proposed [15,16]  $R_e$  value of the  $A(^2\Pi_{u,1/2})$  state,  $\sim 3 \text{ Å}$ , produces a  $B$  value of  $\sim 0.03 \text{ cm}^{-1}$ , much larger than the present value of  $0.013 \text{ cm}^{-1}$ . Thus, the vibrational and rotational constants of the  $A(^2\Pi_{u,1/2})$  state are very different from those of the observed Rydberg state. This points to the Rydberg state being built on a  $^2\Sigma_u^+$  or  $^2\Sigma_u^-$  ionic core, although the assignment must remain tentative. Further insight should be gained by considering the vibrational progression observed here in conjunction with that of another, so far unassigned, core-excited Rydberg state observed previously [8] and that work is currently under way.

#### 4. Conclusions

We have observed a vibrational progression,  $v = 0-27$ , of a previously unknown state in  $\text{I}_2$ . The state has been identified as a  $0_u^+$   $6s$  Rydberg state correlating with  $\text{I}(^2P_{3/2}) + \text{I}^*[^3P_2]_c;6s;^2P_{3/2}$  based on an excited electronic state of the core. Vibrational and rotational constants have been determined and used to calculate the RKR potential function. It is surprising that although the state sits just above the lowest dissociation limit to a  $6s$  Rydberg atomic state, the spectrum consists of regular, sharp features indicating that the state is not perturbed or predissociated, at least up to 70% of  $D_e$ .

#### Acknowledgements

We thank Dr. P.R.R Langridge-Smith for the loan of a dye laser. A.M.S. thanks the Göran Gustafsson foundation for a scholarship.

#### References

- [1] A.J. Yencha, M.C.R. Cockett, J.G. Goode, R.J. Donovan, A. Hopkirk, G.C. King, Chem. Phys. Lett. 229 (1994) 347.
- [2] A. Kvaran, A.J. Yencha, D.K. Kela, R.J. Donovan, A. Hopkirk, Chem. Phys. Lett. 179 (1991) 263.
- [3] T. Ridley, D.A. Beattie, M.C.R. Cockett, K.P. Lawley, R.J. Donovan, Phys. Chem. Chem. Phys. 4 (2002) 1398.
- [4] H. Lefebvre-Brion, K. Yoshino, J. Mol. Spectrosc. 158 (1993) 140.
- [5] Ch. Jungen, K.P. Huber, M. Jungen, G. Stark, J. Chem. Phys. 118 (2003) 4517, and references therein.
- [6] P. Venkateswarlu, Can. J. Phys. 48 (1970) 1055.
- [7] T. Ridley, M. de Vries, K.P. Lawley, S. Wang, R.J. Donovan, J. Chem. Phys. 117 (2002) 7117.

- [8] A.M. Sjödin, T. Ridley, K.P. Lawley, R.J. Donovan, *J. Chem. Phys.* 120 (2004) 2740.
- [9] J.C.D. Brand, A.R. Hoy, A.K. Kalkar, A.B. Yamashita, *J. Mol. Spectrosc.* 95 (1982) 350.
- [10] P. Luc, *J. Mol. Spectrosc.* 80 (1980) 41.
- [11] F. Martin, S. Churassy, R. Bacis, R.W. Field, J. Verges, *J. Chem. Phys.* 79 (1983) 3725.
- [12] C.C. Kiess, C.H. Corliss, *J. Res. Nat. Bur. Std. A* 63 (1959) 1.
- [13] M.C.R. Cockett, R.J. Donovan, K.P. Lawley, *J. Chem. Phys.* 105 (1996) 3347.
- [14] A.B. Cornford, D.C. Frost, C.A. McDowell, J.L. Ragle, I.A. Stenhouse, *J. Chem. Phys.* 54 (1971) 2651.
- [15] J. Li, K. Balasubramanian, *J. Mol. Spectrosc.* 138 (1989) 162.
- [16] W.A. de Jong, L. Visscher, W.C. Nieuwpoort, *J. Chem. Phys.* 107 (1997) 9046.
- [17] A.J. Yench, T. Ridley, R.R.J. Maier, R.V. Flood, K.P. Lawley, R.J. Donovan, A. Hopkirk, *J. Phys. Chem.* 97 (1993) 4582.